Structural Insight into the Binding Diversity between the Human Nck2 SH3 Domains and Proline-Rich Proteins[†,‡]

Jingxian Liu,[§,||] Minfen Li,[||,⊥] Xiaoyuan Ran,[§] Jing-song Fan,[⊥] and Jianxing Song*[,§,⊥]

Department of Biochemistry, Yong Loo Lin School of Medicine, and Department of Biological Sciences, Faculty of Science, National University of Singapore, 10 Kent Ridge Crescent, Singapore 119260

Received January 16, 2006; Revised Manuscript Received April 12, 2006

ABSTRACT: Human Nck2 (hNck2) is a 380-residue adapter protein consisting of three SH3 domains and one SH2 domain. Nck2 plays a pivotal role in connecting and integrating signaling networks constituted by transmembrane receptors such as ephrinB and effectors critical for cytoskeletonal dynamics and remodeling. In this study, we aimed to determine the NMR structures and dynamic properties of the hNck2 SH3 domains and to define their ligand binding preferences with nine proline-rich peptides derived from Wire, CAP-1, CAP-2, Prk, Wrch1, Wrch2, and Nogo. The results indicate (1) the first hNck2 SH3 domain is totally insoluble. On the other hand, although the second and third hNck2 SH3 domains adopt a conserved SH3 fold, they exhibit distinctive dynamic properties. Interestingly, the third SH3 domain has a far-UV CD spectrum typical of a largely unstructured protein but exhibits $\{^1H\}-^{15}N$ steady-state NOE values larger than 0.7 for most residues. (2) The HSQC titrations revealed that the two SH3 domains have differential ligand preferences. The second SH3 domain seems to prefer a consensus sequence of APx#PxR, while the third SH3 domain prefers PxAPxR. (3) Several high-affinity bindings were identified for hNck2 SH3 domains by isothermal titration calorimetry. In particular, the binding of SH3-3 with the Nogo-A peptide was discovered and shown to exhibit a K_d of 5.7 μM. Interestingly, of the three SH3-binding motifs carried by Wrch1, only the middle one was capable of binding SH3-2. Our results provide valuable clues for further functional investigations into the Nck2-mediated signaling networks.

Environmental signals sensed by cells are specifically transmitted into intracellular space via the transmembrane protein receptors by means of protein−protein interactions between the cytoplasmic domains of the receptors and downstream set of intracellular binding partners. Eph receptors, the largest known family of tyrosine kinases with a total of 14 members, modulate the behavior of many cell types by interacting with their membrane-anchored ligands, ephrins. Eph receptors and ephrins have been shown to function at the interface between pattern development and morphogenesis, such as axon guidance, cell migration, segmentation, and angiogenesis (*1*−*6*). The signaling networks mediated by Eph receptors and ephrins are conserved among metazoans, and eight mammalian ephrins have been identified. Ephrins can be grouped into two structural and functional families: ephrinA and ephrinB (*1*−*8*). The Eph−ephrinB-mediated signaling network has been found to be involved in learning and memory formation (*9*), neuronal regeneration (*10*−*12*), and pain processing (*13*), and differential expressions of ephrinB were also correlated with tumorigenesis (*14*, *15*). Moreover, the roles of Eph-ephrin in stem cells, immune function, and blood clotting are also starting to be realized (*6*). Recently, the ephrinB2 extracellular domain was identified as the entry receptor for the Nipah and Hendra viruses (*16*, *17*).

EphrinB and their Eph receptors are all plasma membrane-anchored proteins and are unique in their ability to transmit signals bidirectionally. In the Eph−ephrinB signaling systems, the same Eph and ephrinB proteins can either send or receive signals, depending on the developmental context (*1*−*8*). In this regard, the cytoplasmic tail of the ephrinB proteins plays an integral role in mediating reverse signaling by interacting with intracellular protein binding partners (*7*, *18*, *19*). Tyr phosphorylation of the ephrinB cytoplasmic domain would abolish its well-folded β-hairpin structure and consequently activate the binding with the SH2[1] domain of the Nck2 adapter protein, thus initiating downstream signaling pathways regulating cytoskeleton assembly and remodeling (*7*, *19*−*22*).

[†] This work was supported by Biomedical Research Council of Singapore (BMRC) Grant R-183-000-097-305 and BMRC Young Investigator Award R-154-000-217-305 (to J.S.).

[‡] The structure coordinates of the second and third human Nck2 SH3 domains were deposited in the Protein Data Bank as entries 2FRW and 2FRY, respectively. Their NMR data were also deposited at the BioMagResBank as entries 6978 and 6977, respectively.

* To whom correspondence should be addressed. Phone: (65) 6874-1013. Fax: (65) 6779-2486. E-mail: bchsj@nus.edu.sg.

[§] Department of Biochemistry, Yong Loo Lin School of Medicine.

[||] These authors contributed equally to this work.

[⊥] Department of Biological Sciences, Faculty of Science.

[1] Abbreviations: CNS, Crystallography and NMR System; DTT, dithiothreitol; FPLC, fast performance liquid chromatography; GST, glutathione *S*-transferase; HPLC, high-pressure liquid chromatography; HSQC, heteronuclear single-quantum correlation; IPTG, isopropyl β-D-thiogalactopyranoside; ITC, isothermal titration calorimetry; NMR, nuclear magnetic resonance; NOE, nuclear Overhauser effect; NOESY, nuclear Overhauser effect spectroscopy; PDB, Protein Data Bank; rms, root-mean-square; SH2, Src homology 2; SH3, Src homology 3; TOCSY, total correlation spectroscopy.

10.1021/bi060091y CCC: $33.50
Published on Web 05/17/2006

Table 1: Nine Proline-Rich Peptides Derived from Seven Proteins and Their Interaction with hNck2 SH3 Domains

peptide	sequence	HSQC titration with SH3-2 (1:2 SH3-2:peptide ratio)	HSQC titration with SH3-3 (1:2 SH3-3:peptide ratio)
Wire (308−321)	SNRPPPPARDPPSR	no	no
CAP-1 (731−745)	SATASPQQPQAQQRR	no	no
CAP-2 (311−325)	PTQEKPTSPGKAIEK	no	no
Prk2 (571−585)	EPEPPPAPPRASSLG	no	yes
nWrch1 (4−16)	QQGDPAFPDRCEA	no	no
mWrch1 (13−27)	RCEAPPVPPRRERGG	yes	no
cWrch1 (27−42)	GRGGRGPGEPGGRGRA	no	no
Wrch2 (14−26)	LRAPTPPPRRRSA	yes	yes
Nogo-A (171−181)	STPAAPKRRGS	no	yes

In addition to engagement in ephrinB reverse signaling, it appears that the Nck proteins play a universal role in coordinating the signaling networks critical for organization of actin cytoskeleton, cell movement, or axon guidance, by connecting the cellular surface receptors down to the multiple intracellular signaling networks in a "Tyr(P) → SH2/SH3 → effector" manner (*23*−*27*). The Nck family has two known members (Nck-1 and Nck-2) in human cells and one in *Drosophila* (Dock) (*28*−*30*). The sequences of the two human Nck proteins are 68% identical, and they are exclusively composed of three SH3 domains and one C-terminal SH2 modular domain. The Nck protein functions by using its SH2 domain to bind Tyr-phosphorylated cytoplasmic regions of the transmembrane receptors such as ephrinB, whereas it uses its SH3 domains to recruit proline-rich effecter proteins to tyrosine-phosphorylated kinase or their substrates. The Nck SH2 and SH3 domains share a very high degree of sequence homology within the family but have a relatively low level of identity with other SH3 and SH2 domains, with only ∼40% for the Nck SH2 domains and ∼50% for the SH3 domains (*23*−*30*). Intriguingly, despite a high degree of homology, Nck1 and Nck2 proteins appear to have differential functional profiles as well as distinct binding specificities for their modular domains (*19*, *23*−*27*). For example, the Nck2 SH2 domain was able to bind phosphorylated ephrinB while the Nck1 SH2 domain was not (*19*). Previously, the NMR structure of the hNck2 SH2 domain was determined, and the results demonstrated that the hNck2 SH2 domain does have some unique properties in terms of the three-dimensional structure and electrostatic potential surface (*22*). Therefore, it is also of significant interest to determine the structural, dynamic, and binding properties of the hNck2 SH3 domains. In this study, we aimed to determine the solution structures and dynamic properties of the hNck2 SH3 domains, as well as to further study their binding interactions with nine proline-rich peptides derived from Wire, CAP-1, CAP-2, Prk, Wrch1, Wrch2, and Nogo by use of heteronuclear NMR spectroscopy and isothermal titration calorimetry (ITC).

MATERIALS AND METHODS

De Novo Synthesis of the Genes. To achieve high-level protein expression, DNA fragments encoding hNck2 SH3 domains with *Escherichia coli*-preferred codons were obtained by a PCR-based de novo gene synthesis approach as previously described (*31*) using DNA oligos listed in Table 1 of the Supporting Information. The dissected hNck2 fragments studied here included three isolated SH3 domains, SH3-1 (residues 5−62), SH3-2 (residues 115−171), and SH3-3 (residues 199−257); the fragments spanning residues 5−171 containing SH3-1 and SH3-2, residues 115−257 covering SH3-2 and SH3-3, residues 5−257 with all three SH3 domains, and also the entire hNck2. The obtained DNA segments were subsequently cloned into His-tagged expression vector pET32a (Novagen) with restriction sites shown in Table 1 of the Supporting Information.

Similarly, DNA fragments encoding proline-rich peptides derived from a variety of proteins were also synthesized with the same approach (*31*) with the oligos in Table 1 of the Supporting Information and subsequently cloned into GST expression vector pGEX-4T-1 (Amersham Biosciences). On the basis of previous publications on CAP (*7*, *19*), Prk (*32*), Wire (*33*), and Wrch1 and Wrch2 (*34*−*37*), the proline-rich motifs were selected and are presented in Table 1. The Nogo-A(171−181) peptide was obtained from our systematic screening of all potential SH3-binding motifs in the Nogo molecule (M. Li, J. Liu, and J. Song, data to be published). Interestingly, as seen in Figure 1c, over the region N-terminal to its Cdc42-like domain, the Wrch2 protein contains only one motif over residues 14−26 while the Wrch1 protein has three, namely, the N-terminal nWrch1(4−16), the middle mWrch1(13−27), and the C-terminal cWrch1(27−42) motifs. All DNA constructs were confirmed by automated sequencing prior to recombinant protein expression.

The recombinant hNck2 SH3 domains were overexpressed in *E. coli* strain BL21 cells. Briefly, the cells were cultured at 37 °C to reach an OD_{600} of 0.4, and then IPTG was added to a final concentration of 0.4 mM to induce recombinant protein expression for 12 h at 20 °C. The recombinant SH3-containing proteins were purified by Ni^{2+} affinity chromatography under native conditions followed by in-gel thrombin cleavage to remove the His tag. The released SH3-containing proteins were further purified either by FPLC on a mono-S column or by HPLC on a reverse-phase C_8 column (Vydac). For GST-fused proline-rich peptides, a similar expression procedure was used to obtain GST fusion proteins which were subsequently purified using glutathione−Sepharose (Amersham Biosciences). The peptides were released from the GST fusion proteins by in-gel thrombin cleavage followed by HPLC purifications on a RP-18 column (Vydac). For NMR isotope labeling, recombinant proteins were prepared by growing the cells in M9 medium with additions of $(^{15}NH_4)_2SO_4$ for ^{15}N labeling and $(^{15}NH_4)_2SO_4$ and [^{13}C]-glucose for ^{15}N and ^{13}C labeling, respectively (*22*). The identities of all proteins and peptides described above were verified by MALDI-TOF mass spectrometry.

NMR Sample Preparation and Experiments. All NMR samples of the hNck2 SH3 domains were prepared in a pH

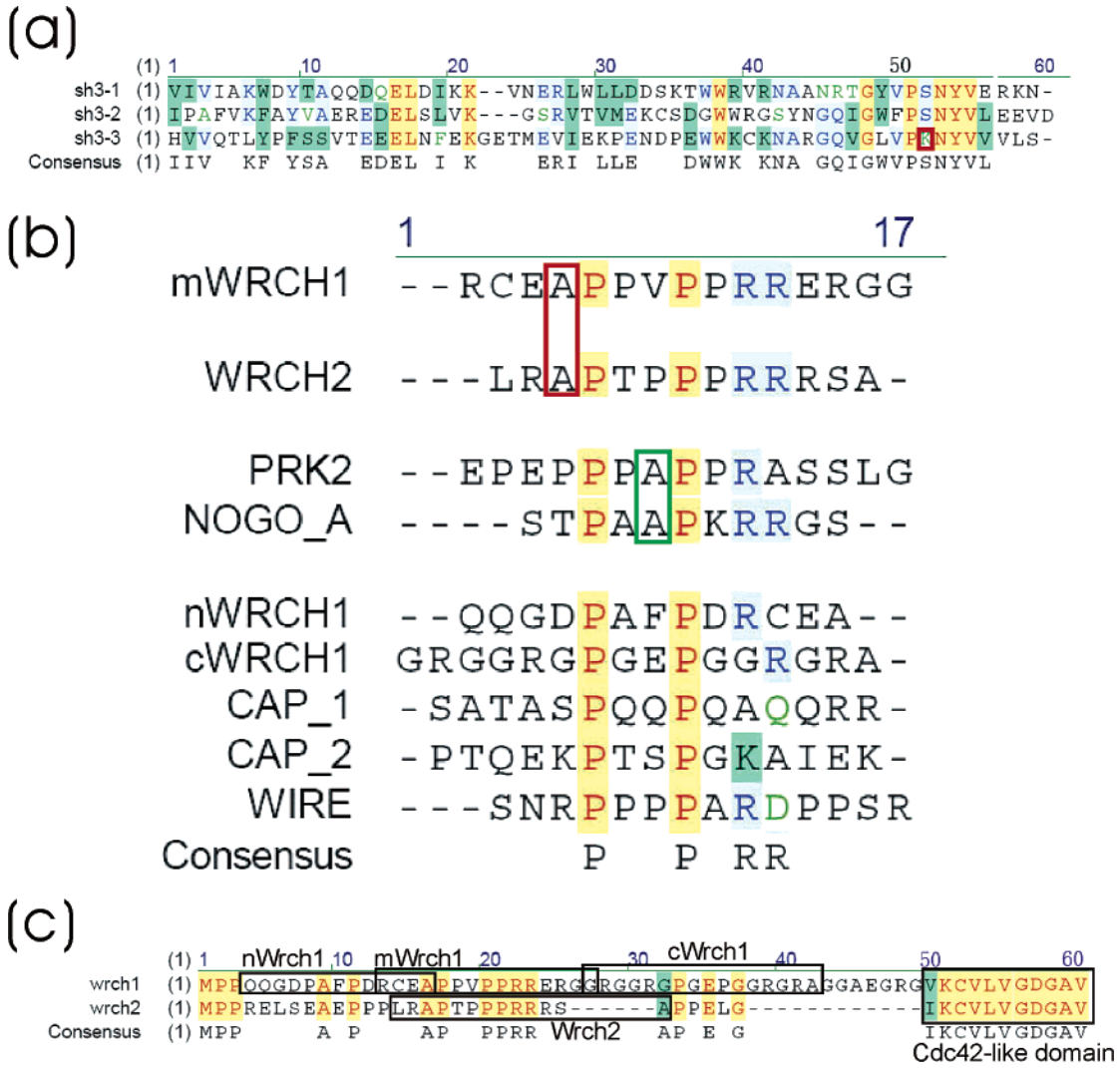

FIGURE 1: Sequence alignments. (a) Amino acid sequences of the three hNck2 SH3 domains, namely, SH3-1, SH3-2, and SH3-3. Lys52, unique in SH3-3, is boxed. (b) Sequence alignment of nine proline-rich SH3 binding motifs studied here which are derived from proteins such as Wrch1, Wrch2, Nogo, CAP-1, CAP-2, and Wire. Their exact locations in the original proteins are indicated in Table 1. The peptides are grouped into four categories: the first group with mWrch1 only capable of binding SH3-2, the third group with Prk2 and Nogo-A only binding SH3-3, the second group with Wrch2 being able to bind both SH3-2 and SH3-3, and the forth group with nWrch1, cWrch1, CAP-1, CAP-2, and Wire showing no significant ability to bind SH3-2 and SH3-3. (c) Sequence alignment of the N-terminal regions unique in Wrch1 and Wrch2, which are not found in other GTPase. The majority of the Wrch1 and Wrch2 Cdc42-like domains have been omitted for clarity. As indicated, Wrch1 contains three proline-rich SH3 binding motifs (nWrch1, mWrch1, and cWrch1) while Wrch2 has only one.

6.8 buffer consisting of 50 mM phosphate, 0.01% (w/v) sodium azide, and 5 mM DTT, with an addition of 10% D_2O for spin lock. The proline-rich peptides were dissolved in the same buffer except that no DTT was added for those containing no cysteine in the sequences. For HCCH-TOCSY and ^{13}C NOESY experiments, the doubly labeled SH3 samples were prepared in a buffer containing 70% D_2O.

NMR experiments were acquired on an 800 MHz Bruker Avance spectrometer equipped with pulse field gradient units at 298 K as described previously (*22*, *38*). Only preliminary HSQC titration screenings were performed on a 500 MHz Bruker Avance spectrometer equipped with both an actively shielded cryoprobe and pulse field gradient units. The NMR spectra acquired for both backbone and side chain assignments included ^{15}N-edited HSQC-TOCSY and HSQC-NOESY as well as triple-resonance experiments [HNCACB, CBCA(CO)NH, HNCO, (H)CC(CO)NH, H(CCO)NH, and HCCH-TOCSY]. NOE restraints for structure calculation were derived from ^{15}N and ^{13}C NOESY spectra. The NOE constraints involved in the aromatic side chains were collected from two-dimensional ^1H NOESY spectra in D_2O. NMR data were processed with NMRPipe (*39*) and analyzed with NMRView (*40*).

NMR Structure Determination. For structure calculation, a set of manually assigned unambiguous NOE restraints together with dihedral angle restraints predicted with TALOS (*41*) based on five chemical shift values (^{15}N, Cα, Cβ, CO, and Hα) was used to calculate initial structures of the human Nck2 SH3 domains with CYANA (*42*). With the availability of the initial structure, more NOE cross-peaks in the two NOESY spectra were automatically assigned with CYANA followed by a manual confirmation. After many rounds of refinement, a final set of unambiguous NOE and dihedral angle restraints were utilized for structure calculations with a simulated annealing protocol implemented in CNS (*22*, *43*, *44*). The 10 lowest-energy structures accepted by the CNS

protocol were checked by PROCHECK (*45*) and subsequently analyzed by using MolMol (*46*) and Pymol (http://www.pymol.org).

Binding Interactions Assessed by HSQC Screening. To characterize the binding interactions between the hNck2SH3 domains and proline-rich peptides listed in Table 1, two-dimensional $^{1}H-^{15}N$ HSQC spectra of the ^{15}N-labeled SH3 domains were acquired at a protein concentration of ~100 μM in the absence or presence of peptides at a molar ratio of ~1:2 (SH3:peptide) as previously described (*22*). If no detectable perturbation of the HSQC peak was observed at this ratio, the peptide was considered to have no significant ability to bind to the SH3 domains, and then no further study was conducted on these peptides. For those with shifted HSQC peaks, the shifted residues were assigned by superimposing the HSQC spectra in the absence and presence of the peptides. The degree of perturbation was measured by an integrated chemical shift index calculated by the formula $[(\Delta^{1}H)^2 + (\Delta^{15}N/4)^2]^{1/2}$ (ppm).

To explore the possibility of extracting the dissociation constant by NMR spectroscopy, the ^{15}N-labeled SH3 domains were HSQC-titrated by gradually adding peptides until the binding was largely saturated. The tracing of the shifted peaks was assigned by superimposing all HSQC titration spectra and subsequently fitted by the script developed by K. Gardner (freedom7.swmed.edu/NMRview/titration.html) to estimate the dissociation constant (K_d).

The binding interaction between the Nogo-A peptide and SH3-3 was further investigated by monitoring the shifts of HSQC peaks of the ^{15}N-labeled Nogo-A peptide upon addition of an excess of the unlabeled SH3-3 domain.

ITC Characterization of the Binding. All ITC calorimetric titrations were performed using a Microcal VP ITC machine (*47*, *48*). The proteins were in 50 mM Tris buffer (pH 7.0), with 3 mM 2-mercaptoethanol. After centrifugation for 15 min, the samples were degassed for 15 min to prevent the formation of bubbles. The protein samples (either second or third SH3 domain) were placed in the ~1.4 mL reaction cell, and the ligand (either mWrch1, Wrch2, or Nogo-A peptide) was loaded into the 300 μL injection syringe. Titrations were performed at 30 °C, and control experiments (peptides titrated into buffer alone) were also conducted to evaluate the heats of dilution. The titration data after subtracting the corresponding blank results were fitted using the built-in software ORIGIN to obtain thermodynamic parameters.

CD and NMR Dynamic Characterization. CD experiments were performed on a Jasco J-810 spectropolarimeter equipped with a thermal controller as described previously (*31*). The far-UV CD spectra of the hNck2 SH3-2 and SH3-3 domains were collected over a wide range of peptide concentrations in 50 mM phosphate buffer (pH 6.8) at 20 °C, using a cuvette with a path length of 1 mm with a spectral resolution of 0.1 nm. The near-UV CD spectra were collected at a protein concentration of 200 μM in the absence and presence of 8 M urea. Data from five independent scans were added and averaged.

^{15}N T_1 and T_2 relaxation times and $\{^{1}H\}-^{15}N$ steady-state NOEs were determined on the 800 MHz spectrometer at 20 °C as described previously (*20*, *49*, *50*). ^{15}N T_1 values were measured from HSQC spectra recorded with relaxation delays of 10, 500, 100, 600, 200, 300, 400, 900, and 700 ms. ^{15}N T_2 values were determined with relaxation delays of 10, 60, 30, 100, 80, 120, 160, and 180 ms. $\{^{1}H\}-^{15}N$ steady-state NOEs were obtained by recording spectra with and without ^{1}H presaturation with a duration of 3 s plus a relaxation delay of 6 s at 800 MHz. The preliminary analysis of the data using the model-free approach was conducted with Modelfree 4.15 (*51*) as well Tensor (*52*).

RESULTS

Gene Synthesis and Protein and Peptide Production. A high protein expression level was achieved in *E. coli* BL21 cells for the de novo-synthesized DNA constructs encoding hNck2 SH3 domains and the proline-rich peptides. Unfortunately, the first hNck2 SH3 domain was found to be totally insoluble in the isolated form, in the forms linked with the second SH3 domain, and even with all three SH3 domains together. On the other hand, the entire 380-residue hNck2 protein was soluble, although it precipitated above a concentration of 1 mg/mL. This indicated that the presence of the C-terminal SH2 domain or/and the loop linking the third SH3 domain to the SH2 domain might enhance the solubility of the first SH3 domain. Moreover, we also conducted extensive assessment of the construct with the second and third SH3 domains connected by the native linker sequence. The HSQC peaks of the isolated SH3-2 domain were almost superimposable with the corresponding region in the linked protein, while SH3-3 peaks underwent slight shifts. We have also labeled this protein with ^{15}N and ^{13}C and collected a series of triple-resonance spectra. Unfortunately, the spectra could not be assigned due to the extensive disappearance of resonance peaks resulting from the conformational exchange on the microsecond to millisecond time scale. However, we compared the binding profiles of the isolated and connected domains with those of the Nogo peptides and found no significant difference (data not shown). Consequently, in this study, we placed our focus on the SH3-2 and SH3-3 domains and have successfully generated ^{15}N-labeled and ^{15}N- and ^{13}C-labeled samples for determination of NMR structures as well as study of their interactions with nine proline-rich peptides as listed in Table 1.

NMR Structure Determination of the Second and Third hNck2 SH3 Domains. As shown in Figure 1a, the hNck2 SH3-2 domain consists of 57 residues while the SH3-3 domain contains 59 residues. For both SH3 domains, backbone assignments were successfully achieved for all non-proline residues with analysis of a pair of triple-resonance experiments, CBCA(CO)NH and HN(CO)CACB, and the assigned HSQC spectra are shown in Figure 2. Side chain carbon and proton assignments were also completed for most residues on the basis of analysis of CCCONH, ^{15}N-edited HSQC-TOCSY, and HCCH-TOCSY spectra. With the input of the dihedral angles predicted by TALOS and NOE distances derived from three-dimensional ^{15}N HSQC-NOESY and ^{13}C NOESY experiments as well as two-dimensional NOESY experiments for aromatic side chain connectivities, the NMR structures of the hNck2 SH3-2 and SH3-3 domains were calculated by the combined use of CYANA and CNS. Table 2 summarizes the constraints used and structural statistics for the 10 lowest-energy NMR structures of both domains accepted by the CNS protocol, with distance violations of <0.2 Å and dihedral angle violations of <5°. Figure 3 shows the superimposition of the 10 selected structures of the SH3-2 and SH3-3 domains. Both hNck2

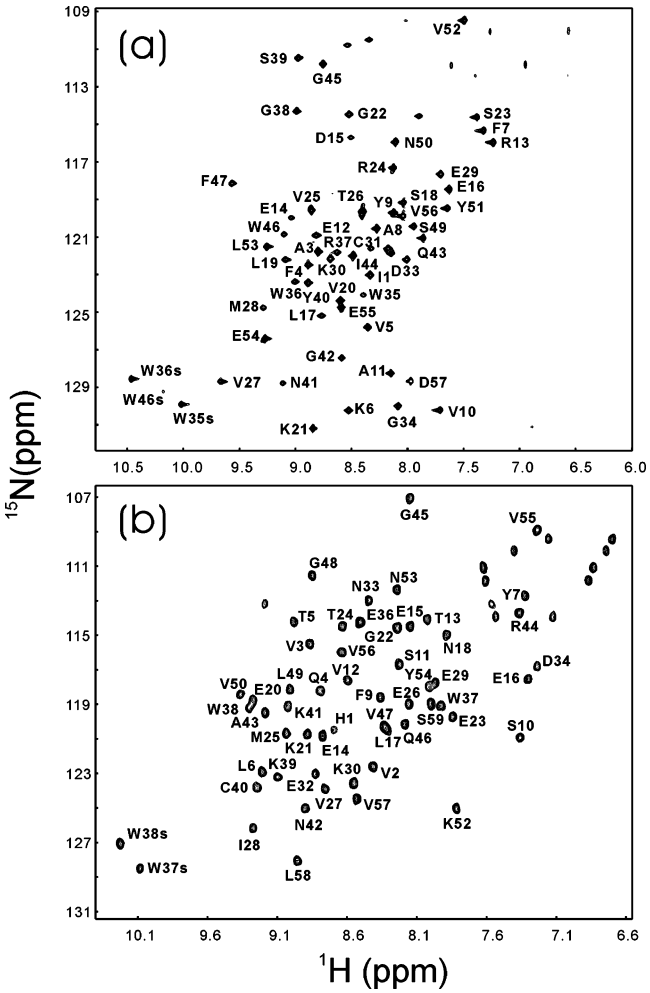

FIGURE 2: NMR sequential assignments. (a) HSQC spectrum of the hNck2 SH3-2 domain. (b) HSQC spectrum of the hNck2 SH3-3 domain. Both spectra were acquired on an 800 MHz NMR spectrometer in 50 mM phosphate buffer (pH 6.8) at 20 °C. The assigned residues are labeled in the spectra.

SH3 domains adopt a conserved tertiary architecture common to all SH3 domains, composed of five β-strands organized into two β-sheets packed at right angles. The first β-sheet is formed by β-strands 1 and 5, together with the first half of β-strand 2, while the second β-sheet is formed by β-strands 3 and 4 and the second half of β-strand 2. Between β-strands 1 and 2 are the long RT loops arranged in an antiparallel manner, and between β-strands 2 and 3 are the shorter n-Src loops (panels a and c of Figure 3). It appears that both RT- and n-Src loops were less defined than the secondary structure regions, as evident from the large backbone rms deviation over these regions (panels b and d of Figure 3). The four-residue fragment led by proline between strands 4 and 5 assumes a 3_{10}-helix characteristic of all SH3 domains.

Figure 3c presents a superimposition of hNck2 SH3-2 and Nck1 SH3-2 domains recently deposited (PDB entry 2CUB). Overall, the two structures are very similar, with a backbone rms deviation of ~1.35 Å over the secondary structure regions despite inclusion of the flexible linker regions in the Nck1 SH3-2 structure. Interestingly, the characteristic 3_{10}-helix is missing in a portion of the Nck1 SH3-2 structures, and the implication of this observation needs to be explored when the detailed description of the Nck1 SH3-2 domain is available. Furthermore, the structure of the hNck2 SH3-3 domain determined here was also compared with that complexed with the LIM4 domain (PDB entry 1U5S), as well as a newly deposited structure (PDB entry 1WX6) (Figure 3f). Although both 1WX6 and 1U5S included extended sequences at both termini, the three structures are very similar, with a pairwise backbone rms deviation of ~1.00 Å over the secondary structure regions. The main difference between the hNck2 SH3-3 structure determined here and 1U5S in complex with the LIM4 domain is over the N- and C-terminal regions, probably because 1U5S is a complex structure which uses a nonclassic region that consists of N- and C-termini to bind LIM4 in an ultraweak manner (with a K_d of 3 mM).

Table 2: NMR Constraints and Structural Statistics for the 10 Lowest-Energy Structures of the Second and Third hNck2 SH3 Domains

	second SH3 domain	third SH3 domain
restraints for calculation		
total NOE restraints	880	722
intraresidue	394	300
sequential	257	175
medium-range	36	47
long-range	193	200
dihedral angel constraints	87	90
final energies (kcal/mol)		
E(total)	171.73 ± 34.15	227.60 ± 31.31
E(bond)	7.47 ± 1.44	11.2 ± 1.12
E(angle)	50.48 ± 6.63	64.42 ± 9.78
E(improper)	8.25 ± 2.24	10.83 ± 3.78
E(van der Waals)	49.21 ± 2.67	87.15.0 ± 15.21
E(NOE)	45.92 ± 7.32	48.84 ± 6.56
root-mean-square deviations from idealized geometry		
bonds (Å)	0.0028 ± 0.00026	0.0040 ± 0.0005
angles (deg)	0.4478 ± 0.029	0.5753 ± 0.068
impropers (deg)	0.3237 ± 0.0431	0.479 ± 0.0872
NOEs (Å)	0.0330 ± 0.0026	0.0451 ± 0.0055
Ramachandran statistics (%)		
most favored	75.4	84.6
additionally allowed	21.2	15.4
generously allowed	2.7	0.0
disallowed	0.0	0.0
root-mean-square deviation from the lowest-energy structure (Å)		
all residues		
all atoms	1.78	1.64
heavy atoms	1.56	1.44
backbone atoms	0.92	0.74
secondary structure regions		
all atoms	1.40	1.24
heavy atoms	1.25	0.95
backbone atoms	0.48	0.37

HSQC Identification of the Residues Involved in Binding of the hNck2 SH3 Domains. The binding interactions between the two SH3 domains and nine proline-rich peptides were first screened by HSQC titration at a molar ratio of 1:2 (SH3: peptide). In fact, five peptides, nWrch1, cWrch1, WIRE, CAP-1, and CAP-2, showed no detectable binding to the second or third SH3 domain. This observation indicates that these peptides may bind the first SH3 domain because they were all previously demonstrated to interact with the Nck2 protein. On the other hand, the mWrch1 peptide was found to specifically bind the SH3-2 domain, while the Nogo-A and Prk2 peptides bind the SH3-3 domain exclusively. Very interestingly, on the basis of HSQC titration, the Wrch2 peptide was able to bind both SH3 domains.

The chemical shift changes induced by peptides at a molar ratio of 1:2 were measured by superimposing the HSQC

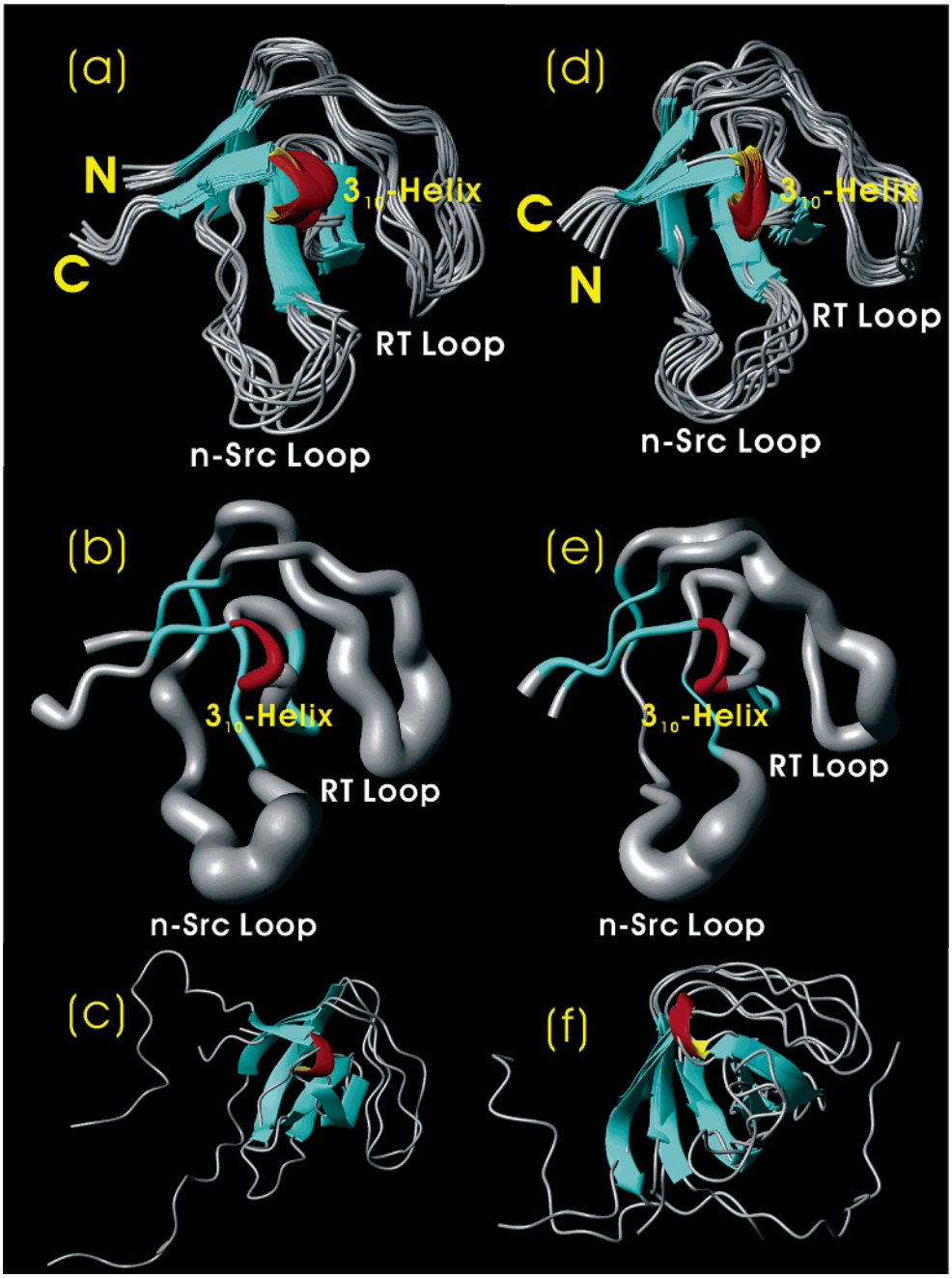

FIGURE 3: Three-dimensional structures as determined by NMR spectroscopy (a and b). Superimposition of the 10 lowest-energy NMR structures of the hNck2 SH3-2 domain in ribbon (a) and sausage (b) modes. (c) Comparison of the structures of the hNck2 SH3-2 domain determined here and deposited Nck1 SH3-2 domain (2CUB). (d and e) Superimposition of the 10 lowest-energy NMR structures of the hNck2 SH3-3 domain in ribbon (d) and sausage (e) modes. (f) Comparison of the structures of the hNck2 SH3-3 domain determined here and 1WX6 with additional extensions, as well as 1U5S complexed with the LIM4 domain. Three characteristic regions previously established to be critical for binding affinity and specificity are indicated, namely, the RT-Src loop, the n-Src loop, and the 3_{10}-helix.

spectra of the SH3 domains in the free state and in the presence of the peptides as shown in Figure 4. In general for both SH3 domains, the significantly affected residues were located over three regions, namely, the RT loop, the n-Src loop, and the 3_{10}-helix, consistent with the previously accepted notion that both the affinity and the specificity of the SH3−ligand interaction are mainly mediated by an interfacial region constituted by residues scattered over these three regions. However, a closer examination revealed that the two SH3 domains have distinctive sets of binding-perturbed residues. As shown in Figure 5a, for the SH3-2 domain, the significantly affected residues included Val5, Phe7, Arg13, Asp15, and Glu16 on the RT loop, Lys30, Cys31, and Gly34 on the n-Src loop, and Phe47, Ser49, and Tyr51 close to or on the 3_{10}-helix. However, for SH3-3, the most-perturbed residues were Thr13 and Glu14 on the RT loop, Glu32, Asn33, and Asp34 on the n-Src loop, and Lys52 on the 3_{10}-helix. It appears that for SH3-2, more hydrophobic residues were involved in ligand binding, while for SH3-3, more hydrophilic, particularly negatively charged residues such as Asp and Glu were engaged in binding. Interestingly, upon introduction of the Wrch2 peptide capable of binding both SH3 domains, the most drastically perturbed residues were located on the 3_{10}-helix, namely, a hydrophobic/

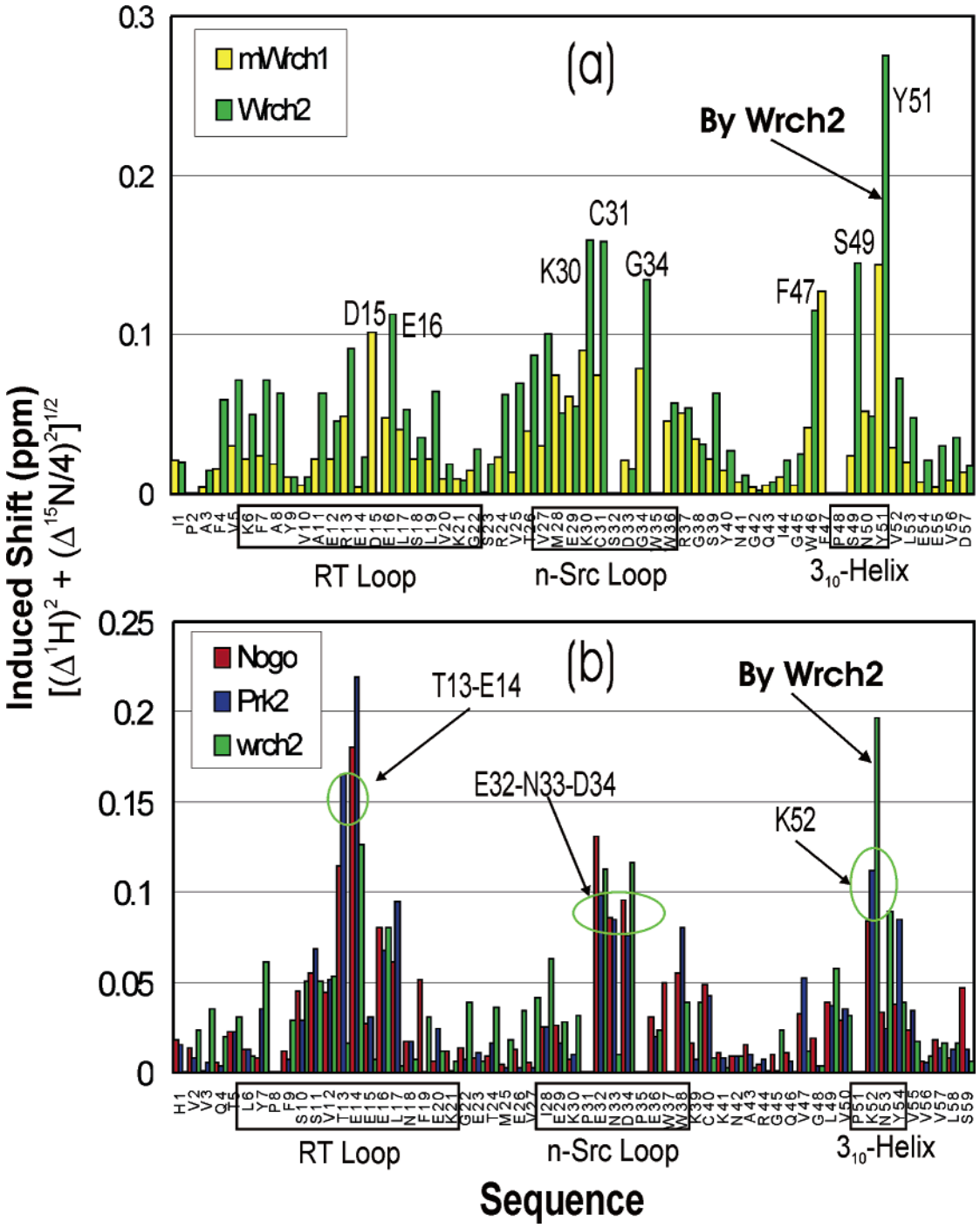

FIGURE 4: Residue specific chemical shift changes induced by ligand binding. Binding-induced chemical shift changes of the HSQC peaks at a molar ratio of 1:2 (SH3:peptide): (a) SH3-2 with addition of mWrch1 (yellow bars) and Wrch2 peptides (green bars) and (b) SH3-3 with addition of Nogo-A (red bars), Prk2 (blue bars), and Wrch2 peptides (green bars). The regions including RT- and nSrc-loops and the 3_{10}-hlix typical of SH3 domains are boxed, and significantly affected residues are labeled. In particular, upon addition of Wrch2, the most significantly affected residue is labeled, namely, Tyr51 of SH3-2 and Lys52 of SH3-3.

aromatic residue (Tyr51) for SH3-2 and a positively charged residue (Lys52) for SH3-3.

For binding-active peptides at a molar ratio of 1:2 (SH3: peptide), further titrations were conducted by gradually increasing the peptide concentration to explore the possibility to determine the dissociation constant, K_d, by fitting HSQC peak tracings. However, it turned out that the binding landscape as detected by HSQC titration of the two SH3 domains was very complex. First, some HSQC peaks started to disappear when the peptide concentration reached a certain point. Second, for some HSQC peaks which could be followed over the whole titration, it was impossible to fit their tracings by a two-site model, indicating that other mechanisms might also be involved. Third, the obtained K_d values varied in a large range and were universally weaker than those obtained by ITC (data not shown). Our results are in a good agreement with a previous report in which this phenomenon was explained by the speculation that NMR detection was too sensitive to other unspecific processes such as binding-induced dynamic changes (*53*).

To gain further insight into the binding of the Nogo-A peptide with SH3-3 identified in this study, we labeled the

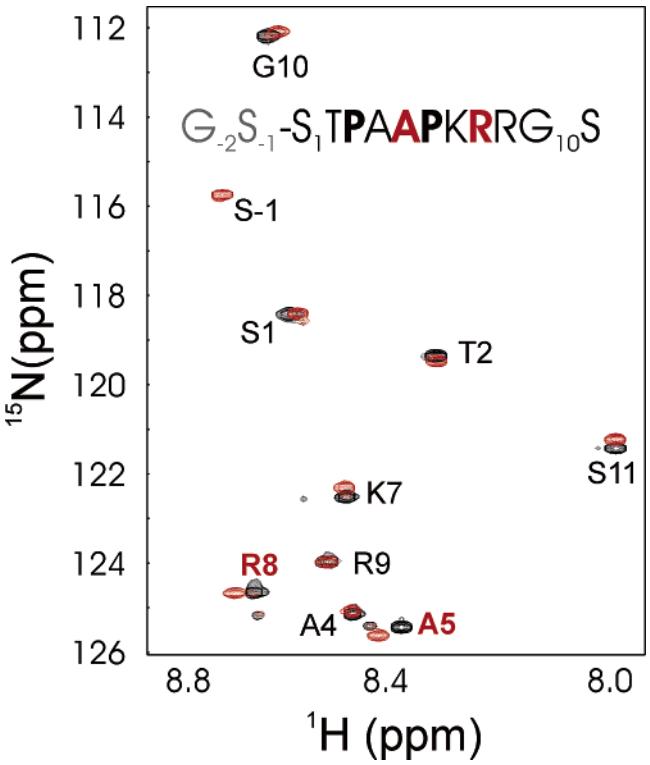

FIGURE 5: Binding of the ^{15}N-labeled Nogo-A peptide with the hNck2 SH3-3 domain. Superimposition of the HSQC spectra of the ^{15}N-labeled Nogo-A peptide in the absence (black) and presence of the hNck2 SH3-3 domain (red) at a molar ratio of 1:3 (peptide: SH3-3). Both spectra were acquired in 50 mM phosphate buffer (pH 6.8) at 20 °C on an 800 MHz NMR spectrometer. The sequential assignments of Nogo-A peptide were determined by analyzing heteronuclear HSQC-TOCSY and HSQC-NOESY spectra. The sequence of the Nogo-A peptide was included, and the two most significantly affected residues, Ala5 and Arg9, upon binding are colored red. $G_{-2}S_{-1}$ was used to indicate the two non-Nogo residues left over from thrombin cleavage of the GST fusion protein.

Nogo-A peptide with ^{15}N and subsequently monitored its HSQC peak shifts induced by adding an excess of the unlabeled SH3-3 domain. The results indicated that upon binding the majority of the HSQC peaks shifted (Figure 5). In particular, HSQC peaks of Ala5 and Arg8 were significantly shifted. As judged from its sequence, Nogo-A peptide belongs to the class II SH3 ligands which have a consensus sequence of xPx#PxR (*54*−*61*). While x can be any amino acid, # is a hydrophobic residue (usually Leu, Pro, or Val). To this end, the significant shift of the Arg8 peak was anticipated because this residue was thought to play a critical role in binding with SH3 domains. By contrast, Ala5 with a dramatic peak shift was not commonly found at that position of the class II ligands. Interestingly, Prk2, another high-affinity ligand for the hNck2 SH3-3 domain, also has an Ala at that position (Figure 1b). This observation implied that the Ala residue at this position might play an important role in specifying the ligand preference for the hNck2 SH3-3 domain.

Thermodynamic Binding Parameters. To quantitatively characterize the binding interactions, we conducted further ITC titration studies on the binding of SH3-2 to mWrch1 and Wrch2, as well as the binding of SH3-3 to Nogo-A and Wrch2. Figure 6 presents the ITC titration data after subtraction of the blank titration results. Except for the result with the SH3-3−Wrch2 interaction (Figure 6d) which gave rise to a very unusual profile, the remaining data could be fitted to generate thermodynamic binding parameters listed in Table 3. All three binding interactions exhibit similar affinities, with K_d values of 9.8 μM for the SH3-2−mWrch1 interaction, 5.0 μM for the SH3-2−Wrch2 interaction, and 5.7 μM for the SH3-3−Nogo-A interaction. Unfortunately, we were unable to fit the unusual ITC result for the SH3-3−Wrch2 interaction (Figure 6d) to output reliable parameters. By using NMR HSQC titrations, its dissociation constant, K_d, was estimated to be >200 μM.

CD and NMR Dynamic Characterization. Far-UV CD spectra for both SH3 domains were acquired in the same buffer for NMR experiments (Figure 8a). Very surprisingly, SH3-3 has a spectrum with the maximal negative signal close to 200 nm and no positive signal around 190 nm, indicating that the SH3-3 is largely unstructured if based on the CD result (*62*). However, this interpretation totally disagrees with the NMR results which show that SH3-3 has a well-dispersed HSQC spectrum (Figure 2a) as well as a large amount of long-range NOE connectivities comparable to those of a well-folded protein. Furthermore, the far-UV CD spectra of the SH3-3 domain were collected at a large range of protein concentrations, and no significant concentration dependence was observed, indicating no significant aggregation of SH3-3 occurred. To understand this phenomenon, near-UV CD spectra were acquired for SH3-2 (Figure 8b) and SH3-3 (Figure 8c) in the absence and presence of 8 M urea. The significant difference between the spectra under the native condition and 8 M urea indicated that like SH3-2, SH3-3 also has a very tight tertiary packing, consistent with the presence of very upfield NMR signals at ca. −0.5 ppm in the one-dimensional ^{1}H NMR spectrum (spectrum not shown). However, the SH3-3 domain was thermodynamically unstable because a portion of the protein was unfolded if the sample was exposed to an acidic pH or kept at 4 °C for more than 2 weeks. Moreover, the possible aggregations of both SH3 domains were also assessed by monitoring HSQC peaks at different protein and DTT concentrations, but no significant changes in chemical shifts and line widths were observed, again indicating no detectable aggregation.

To further assess this unusual observation, ^{15}N backbone relaxation data were collected for both SH3-2 (Figure 9) and SH3-3 (Figure 10). ^{15}N NMR backbone relaxation data provide valuable information about the dynamics of the local environment of a protein on the picosecond to nanosecond time scale (*49*−*52*). In particular, {^{1}H}−^{15}N heteronuclear steady-state NOE (hNOE) provides a measure of backbone flexibility. As seen from Figures 9 and 10, both SH3 domains have hNOE values larger than 0.7 for most residues, indicating that both domains have a significant limitation for backbone motions. However, if compared with SH3-2 which had an average T_2 value of ∼100 ms (Figure 9b), SH3-3 had a much shorter average T_2 value of ∼80 ms (Figure 10b), implying that it might undergo conformational exchanges on the microsecond to millisecond time scale and/or dynamic aggregation which was not detected by CD and HSQC experiments. Consistent with T2 data, the HSQC peaks of SH3-3 were much broader than those of SH3-2 (Figure 2). The line broadening might reduce the signal:noise ratio of HSQC peaks and consequently make the measure-

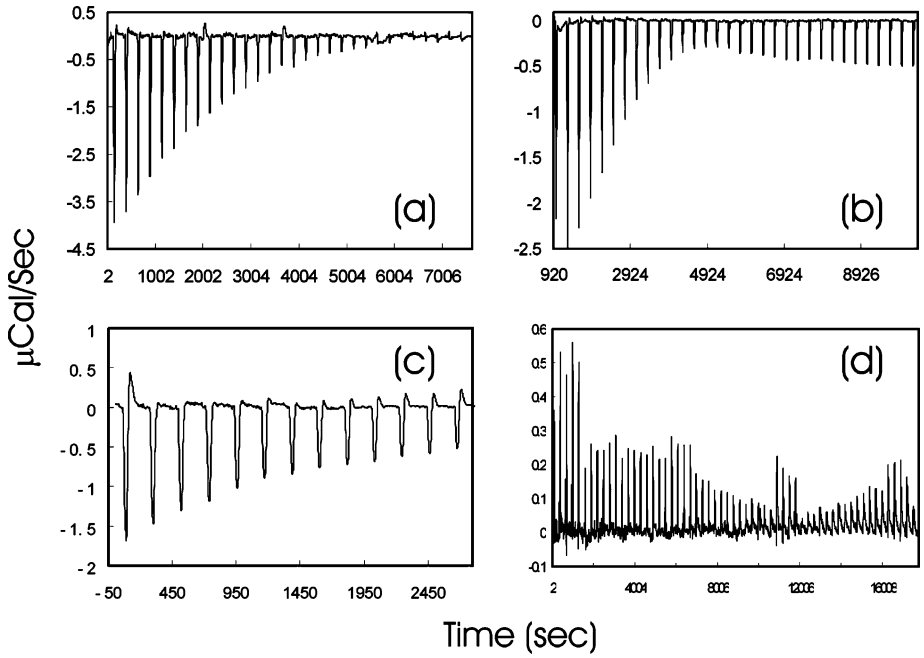

FIGURE 6: ITC characterization. The titration profiles of four binding interactions after subtraction of the corresponding blank results. (a) Interaction between SH3-2 and mWrch1. (b) Interaction between SH3-2 and Wrch2. (c) Interaction between SH3-3 and Nogo-A peptide. (d) Interaction between SH3-3 and Wrch2. The detailed conditions of the ITC experiments are given in Materials and Methods.

Table 3: Thermodynamic Parameters of the Binding Interactions between mWrch1 and hNck2 SH3-2 and between Nogo-A Peptide and hNck2 SH3-3 As Measured by ITC

syringe	cell	buffer	each injection	K_a (M^{-1})	K_d (μM)	stoichiometry (n)	ΔS (cal/mol)	ΔH (cal/mol)
mWrch1 (13−27) (0.58 mM)	SH3-2 (25 μM)	Tris (50 mM, pH 7.0)	5 μL	$1.02 \times 10^5 \pm 5.7 \times 10^3$	9.8	1.01 ± 0.02	−115	$-4.17 \times 10^4 \pm 1.09 \times 10^3$
Wrch2 (14−26) (1.0 mM)	SH3-2 (50 μM)	Tris (50 mM, pH 7.0)	5 μL	$2.0 \times 10^5 \pm 2.54 \times 10^4$	5.0	0.96 ± 0.08	−34.2	$-1.77 \times 10^4 \pm 1.79 \times 10^3$
Nogo-A (171−181) (1.0 mM)	SH3-3 (50 μM)	Tris (50 mM, pH 7.0)	10 μL	$1.75 \times 10^5 \pm 2.3 \times 10^4$	5.7	0.98 ± 0.05	6.7	-5155 ± 482

ment of SH3-3 relaxation data less accurate. This may explain the observation that for SH3-3, T_1 values were more uniform while hNOE data were less uniform (Figure 10).

We have attempted to fit the data for both domains with Modelfree 4.15 as well as Tensor. For the SH3-2 domain, the fitting process even with an isotropic model generated very reasonable order parameters with values larger than 0.8 for many residues, indicating that SH3-2 is well-packed. By contrast, the fitting of the SH3-3 data with different models (isotropic, axially symmetric, and fully asymmetrical) all yield strange results with low order parameters (maximum of ~0.3) and large exchange terms. We also tried to fit the data by initially varying isotropic correlation times, but no significant improvement was obtained. On the other hand, the SH3-3 domain could not be a stable dimer because its T_1 values were totally comparable to those of the SH3-2 domain.

Previously, the drkN SH3 domain was shown to undergo a slow conformational exchange between folded and unfolded and gave rise to two sets of HSQC peaks (*63*). However, in this case, only one set of peaks was detected, indicating that the conformational exchanges of SH3-3 was faster than the NMR time scale. To the best of our knowledge, our results represent the first report showing that a protein could have a far-UV CD spectrum characteristic of an unstructured protein on one hand but have very high hNOE values for most residues. Interestingly, by using hydrogen exchange mass spectrometry, a newly available report demonstrated that SH3 domains exhibit extremely diverse dynamics, and in particular, the underlying mechanism still remains poorly understood (*64*).

To clarify the dynamic mechanism for this unusual observation, extensive investigations are certainly needed in the future which may require ^{15}N backbone relaxation data at several magnetic fields as well as other NMR methods (*63*, *65*, *66*).

DISCUSSION

Multiprotein signaling complexes play a central role in activating, assembling, and propagating intracellular signaling, and the malfunction of such complexes has been directly associated with various human diseases, including cancer, diabetes, and autoimmune and cardiovascular disorders (*67*−*69*). Formation of the complex requires dynamic protein−protein interactions involved in transmembrane

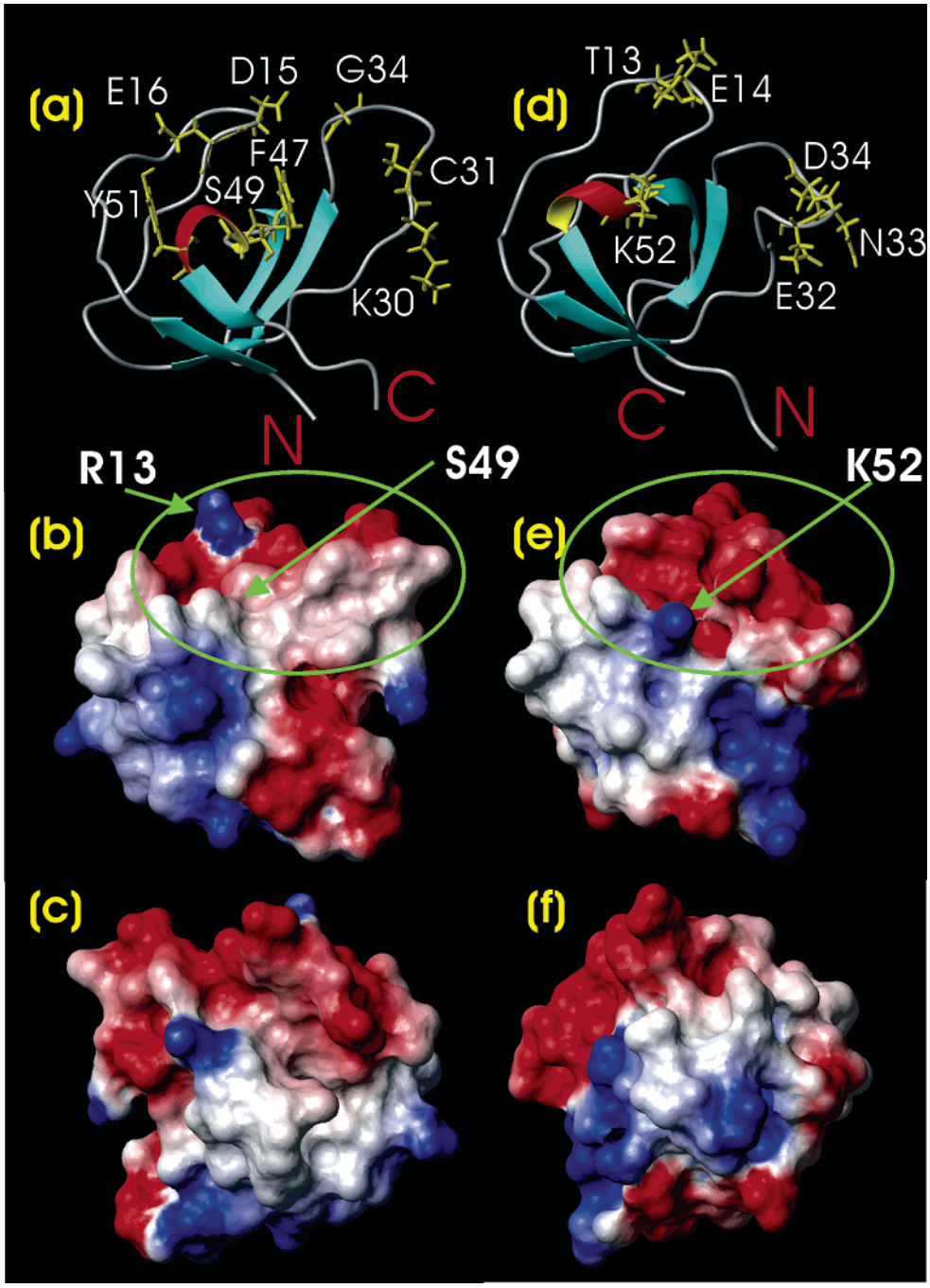

FIGURE 7: Ligand binding and electrostatic potential surfaces. The significantly perturbed residues as identified in Figure 5 are mapped back to the ribbon structures of the hNck2 SH3-2 (a) and SH3-3 (d) domains. Electrostatic potential surfaces of the SH3-2 domain (b) with an orientation exactly the same as that in panel a and (c) with a 180° *y*-axis rotation of panel b. Electrostatic potential surfaces of the SH3-3 domain (e) with an orientation exactly the same as that in panel d and (f) with a 180° *y*-axis rotation of panel e.

receptors, adapter proteins, and effectors and is particularly modulated by interactions between discrete adapter modular domains and specific binding motifs on signaling molecules (*70*−*77*). One nice example of adapter proteins is Nck2 solely composed of three SH3 domains and one SH2 domain which is at a pivotal position for connecting signals from transmembrane receptor kinases down to the effectors, as well as integrating different cellular signaling networks. SH3 domains are probably the most abundant modular domains identified so far, small but vital in the assembly of many intracellular signaling complexes and pathways via dynamic interactions with proline-rich motifs (*54*−*61*). Now it is estimated that more than 400 SH3 domains exist in the human genome and ~25 in the yeast genome (*57*, *60*).

In this study, we found that the first hNck2 SH3 domain was totally insoluble, and consequently, we determined the structures and dynamic properties as well as the binding profiles of the second and third SH3 domains by heteronuclear NMR spectroscopy and ITC. Although both hNck2 SH3 domains adopt the conserved tertiary fold common to all SH3 domains (Figure 3), they have different dynamic properties. The SH3-2 domain is well-structured as indicated by CD spectra and NMR data. Surprisingly the SH3-3 domain has a far-UV CD spectrum characteristic of a largely unstructured protein but exhibits high hNOE values on the

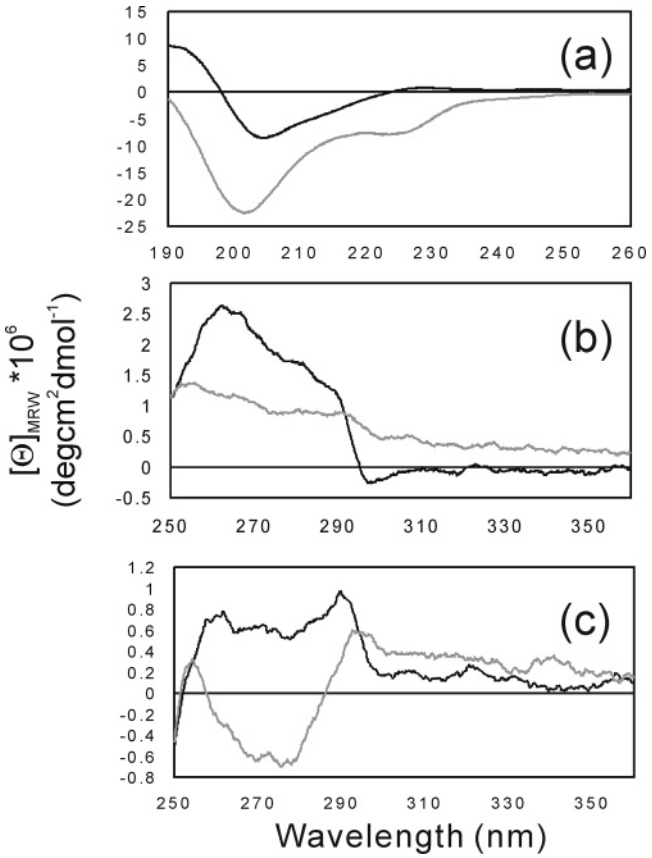

FIGURE 8: CD characterization of the hNck2 SH3-2 and SH3-3 domains. (a) Far-UV CD spectra of hNck2 SH3-2 (black) and SH3-3 (gray) which were collected at a protein concentration of 20 μM in 50 mM phosphate buffer (pH 6.8) at 20 °C on a Jasco J-810 spectropolarimeter. (b) Near-UV CD spectra of hNck2 SH3-2 in the absence (black) and presence of 8 M urea (gray). (c) Near-UV CD spectra of hNck2 SH3-3 in the absence (black) and presence of 8 M urea (gray). The near-UV spectra were collected at a protein concentration of 200 μM in 50 mM phosphate buffer (pH 6.8) at 20 °C.

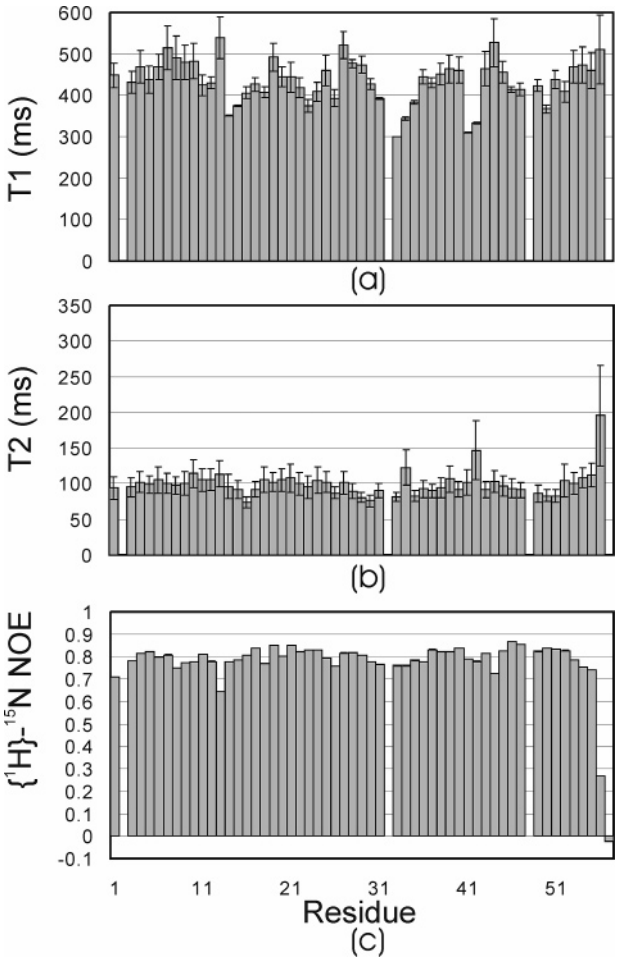

FIGURE 9: ^{15}N NMR backbone relaxation of the hNck2 SH3-2 domain. The ^{15}N NMR backbone relaxation data of the hNck2 SH3-2 domain in 50 mM phosphate buffer (pH 6.8) at 20 °C on an 800 MHz Bruker Avance NMR spectrometer: (a) ^{15}N T_1 (longitudinal) relaxation times, (b) ^{15}N T_2 (transverse) relaxation times, and (c) {^{1}H}−^{15}N steady-state NOE intensities.

other hand. Obviously, this is a very interesting phenomenon that needs to be subjected to extensive dynamic investigations in the future.

On the basis of the HSQC titrations with a group of proline-rich peptides, significantly perturbed residues have been identified (Figure 5) and subsequently mapped back to both SH3 domains (Figure 7). As shown in panels a and d of Figure 7, the residues involved in binding are scattered over the RT- and n-Src loops and the 3_{10}-helix, thus clearly indicating that all binding-active peptides studied here would interact with the conserved ligand-binding surfaces as established for almost all SH3 domains (*54*−*61*). Very interestingly, previously it was demonstrated that the Nck2 SH3-3 domain was also able to utilize a nonclassic and small interface constituted by two terminal residues to interact with the forth LIM domain of PINCH1 at an ultraweak affinity (with a K_d of ∼3 mM) (*78*, *79*). On the other hand, the HSQC titrations also revealed differential ligand preferences for the two SH3 domains. Out of nine peptides that were tested, five have no significant binding to either of the two SH3 domains. Moreover, although the four binding-active peptides all belong to the class II SH3 ligands with a consensus sequence of xPx#PxR (*54*−*61*, *76*, *77*), the two SH3 domains have distinctive preferences for them. Interestingly, mWrch1 and Wrch2 peptides which are able to bind SH3-2 with a high affinity both have an Ala residue N-terminal to the first conserved Pro residue (Figure 1b). On the other hand, peptides Prk2 and Nogo-A binding to SH3-3 have an Ala residue N-terminal to the second conserved Pro residue. The involvement of this Ala in binding is strongly highlighted by the observation that its HSQC peak underwent a dramatic shift upon binding with SH3-3 (Figure 5). This is an interesting result because for most class II ligands, this position is universally occupied by a large hydrophobic residue such as Leu, Pro, or Val. Therefore, it appears that the second hNck2 SH3 domain prefers a ligand with a consensus sequence of APx#PxR, while the third SH3 domain prefers PxAPxR. To gain insight into the rationale for the observed ligand preferences, we analyzed the electrostatic potential surfaces of the two SH3 domains. Interestingly, the SH3-2 ligand-binding surface is composed of both neutral and negatively charged regions, with a small positively charged spot from the Arg13 side chain (Figure 7b). By contrast, the SH3-3 one is strongly dominated by a large and continuous negatively charged area (Figure 7e). It is also worthwhile to note that the 3_{10}-helix residue immediately after the characteristic Pro residue is Ser49 in SH3-2 but Lys52 in SH3-3 (Figure 1a). However, at present,

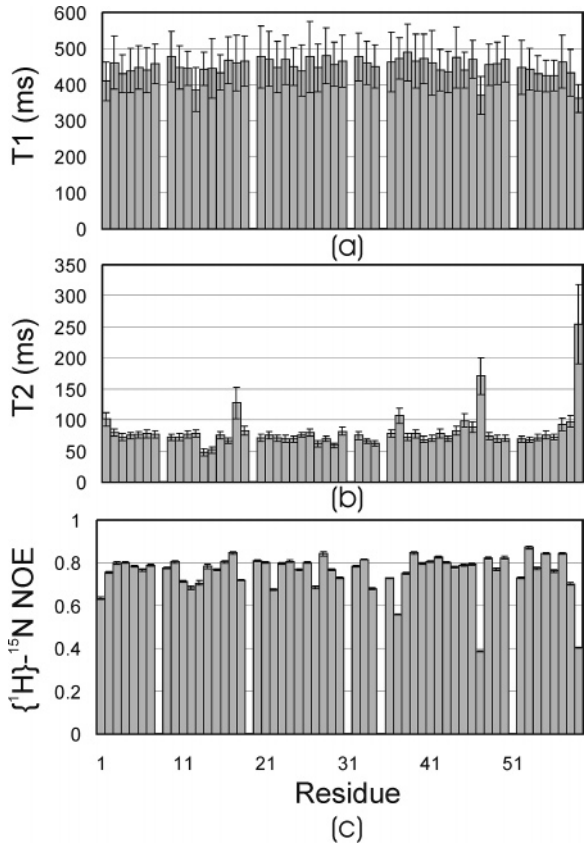

FIGURE 10: ^{15}N NMR backbone relaxation of the hNck2 SH3-3 domain. The ^{15}N NMR backbone relaxation data of the hNck2 SH3-3 domain in 50 mM phosphate buffer (pH 6.8) at 20 °C on an 800 MHz Bruker Avance NMR spectrometer: (a) ^{15}N T_1 (longitudinal) relaxation times, (b) ^{15}N T_2 (transverse) relaxation times, and (c) $\{^1H\}-^{15}N$ steady-state NOE intensities.

fully understanding the determinants of SH3−ligand binding specificity remains a fundamental challenge, partly due to their relatively low binding affinity and promiscuous specificity, with dissociation constants in the micromolar range. For example, although extensive structural determinations of the SH3−ligand complexes revealed that the core interactions are predominantly hydrophobic, formed between conserved SH3 aromatic residues and proline and hydrophobic residues of the ligand, it is still challenging to predict the preference of non-proline residues critical for the binding affinity and specificity as well as to rationalize the binding energetics obtained by thermodynamic studies (*80*, *81*). In this regard, to clarify determinants of the affinity and specificity for the hNck2 SH3 domains, extensive studies by combining site-directed mutagenesis and randomized peptide library approaches are certainly needed in the future.

Recently, Wrch1 and Wrch2 proteins were shown to constitute a novel GTPase subfamily unique in the processing of an extra N-terminal region containing SH3-binding motifs as well as a Cdc42-like domain without any GTPase activity. Although previously the Wrch1 N-terminus has been functionally associated with Grb2 and Nck2 (*34*, *37*), which of the three Wrch1 motifs binds Nck2 remains unknown as does the binding affinity. Now our study clearly reveals that the middle motif of Wrch1 and the only motif contained in Wrch2 were able to bind the hNck2 SH3-2 domain with a similar affinity (with a K_d of 5.0 μM for Wrch2 and 9.8 μM for mWrch1). On the other hand, as Nogo molecules are part of our research focus (*82*), we have examined the Nogo-A sequence and found an extremely interesting fact that within the first 200 residues, a total of 47 proline residues exist and several proline-rich sequences appear to be typical SH3-binding motifs. Therefore, we have systematically investigated the binding between the two hNck2 SH3 domains and these motifs that finally led to the identification of the Nogo-A peptide over residues 171−181 being capable of binding Nck2 (M. Li, J. Liu, and J. Song, data to be published). Here we demonstrate that this Nogo-A peptide can bind to the hNck2 SH3-3 domain with a high affinity (K_d = 5.7 μM). Interestingly, it appears that signaling networks mediated by Nogo and by ephrinB-Nck2 have some overlapped functions, although the underlying mechanism has not yet been discovered (*11*, *12*, *83*, *84*). To this end, our identification of the hNck2−Nogo interaction may provide a valuable clue for further study into its role in neuronal development, regeneration, and tumorigenesis (*85*, *86*).

ACKNOWLEDGMENT

We thank the two anonymous reviewers for their comments, which helped to improve the manuscript significantly; and Dr. Daiwen Yang at the Department of Biological Sciences, National University of Singapore, for fruitful discussion about NMR dynamics.

SUPPORTING INFORMATION AVAILABLE

DNA oligos used to clone hNCK2 SH3 domains and peptides. This material is available free of charge via the Internet at http://pubs.acs.org.

REFERENCES

1. Holder, N., and Klein, R. (1999) Eph receptors and ephrins: Effectors of morphogenesis, *Development 126*, 2033−2044.
2. Flanagan, J. G., and Vanderhaeghen, P. (1998) The ephrins and Eph receptors in neural development, *Annu. Rev. Neurosci. 21*, 309−345.
3. Poliakov, A., Cotrina, M., and Wilkinson, D. G. (2004) Diverse roles of eph receptors and ephrins in the regulation of cell migration and tissue assembly, *Dev. Cell 7*, 465−480.
4. Murai, K. K., and Pasquale, E. B. (2003) 'Eph'ective signaling: Forward, reverse and crosstalk, *J. Cell Sci. 116*, 2823−2832.
5. Gauthier, L. R., and Robbins, S. M. (2003) Ephrin signaling: One raft to rule them all? One raft to sort them? One raft to spread their call and in signaling bind them? *Life Sci. 74*, 207−216.
6. Pasquale, E. B. (2005) Eph receptor signalling casts a wide net on cell behaviour, *Nat. Rev. Mol. Cell Biol. 6*, 462−475.
7. Cowan, C. A., and Henkemeyer, M. (2002) Ephrins in reverse, park and drive, *Trends Cell Biol. 12*, 339−346.
8. Himanen, J. P., and Nikolov, D. B. (2003) Eph signaling: A structural view, *Trends Neurosci. 26*, 46−51.
9. Murai, K. K., and Pasquale, E. B. (2002) Can Eph receptors stimulate the mind? *Neuron 33*, 159−162.
10. Fournier, A. E., and Strittmatter, S. M. (2001) Repulsive factors and axon regeneration in the CNS, *Curr. Opin. Neurobiol. 11*, 89−94.
11. Sandvig, A., Berry, M., Barrett, L. B., Butt, A., and Logan, A. (2004) Myelin-, reactive glia-, and scar-derived CNS axon growth inhibitors: Expression, receptor signaling, and correlation with axon regeneration, *Glia 46*, 225−251.
12. Benson, M. D., Romero, M. I., Lush, M. E., Lu, Q. R., Henkemeyer, M., and Parada, L. F., (2005) Ephrin-B3 is a myelin-based inhibitor of neurite outgrowth, *Proc. Natl. Acad. Sci. U.S.A. 102*, 10694−10699.
13. Battaglia, A. A., Sehayek, K., Grist, J., McMahon, S. B., and Gavazzi, I. (2003) EphB receptors and ephrin-B ligands regulate

spinal sensory connectivity and modulate pain processing, *Nat. Neurosci. 6*, 339−340.
14. Dodelet, V. C., and Pasquale, E. B. (2000) Eph receptors and ephrin ligands: Embryogenesis to tumorigenesis, *Oncogene 19*, 5614−5619.
15. Surawska, H., Ma, P. C., and Salgia, R. (2004) The role of ephrins and Eph receptors in cancer, *Cytokine Growth Factor Rev. 15*, 419−433.
16. Bonaparte, M. I., Dimitrov, A. S., Bossart, K. N., Crameri, G., Mungall, B. A., Bishop, K. A., Choudhry, V., Dimitrov, D. S., Wang, L. F., Eaton, B. T., and Broder, C. C. (2005) Ephrin-B2 ligand is a functional receptor for Hendra virus and Nipah virus, *Proc. Natl. Acad. Sci. U.S.A. 102*, 10652−10657.
17. Negrete, O. A., Levroney, E. L., Aguilar, H. C., Bertolotti-Ciarlet, A., Nazarian, R., Tajyar, S., and Lee, B. (2005) EphrinB2 is the entry receptor for Nipah virus, an emergent deadly paramyxovirus, *Nature 436*, 401−405.
18. Lu, Q., Sun, E. E., Klein, R. S., and Flanagan, J. G. (2001) Ephrin-B reverse signaling is mediated by a novel PDZ-RGS protein and selectively inhibits G protein-coupled chemoattraction, *Cell 105*, 69−79.
19. Cowan, C. A., and Henkemeyer, M. (2001) The SH2/SH3 adaptor Grb4 transduces B-ephrin reverse signals, *Nature 413*, 174−179.
20. Song, J., Vranken, W., Xu, P., Gingras, R., Noyce, R. S., Yu, Z., Shen, S. H., and Ni, F. (2002) Solution structure and backbone dynamics of the functional cytoplasmic subdomain of human ephrin B2, a cell-surface ligand with bidirectional signaling properties, *Biochemistry 41*, 10942−10949.
21. Song, J. (2003) Tyrosine phosphorylation of the well packed ephrinB cytoplasmic β-hairpin for reverse signaling. Structural consequences and binding properties, *J. Biol. Chem. 278*, 24714−24720.
22. Ran, X., and Song, J. (2005) Structural insight into the binding diversity between the Tyr-phosphorylated human ephrinBs and Nck2 SH2 domain, *J. Biol. Chem. 280*, 19205−19212.
23. McCarty, J. H. (1998) The Nck SH2/SH3 adaptor protein: A regulator of multiple intracellular signal transduction events, *BioEssays 20*, 913−921.
24. Buday, L. (1999) Membrane-targeting of signalling molecules by SH2/SH3 domain-containing adaptor proteins, *Biochim. Biophys. Acta 1422*, 187−204.
25. Li, W., and She, H. (2000) The SH2 and SH3 adapter Nck: A two-gene family and a linker between tyrosine kinases and multiple signaling networks, *Histol. Histopathol. 15*, 947−955.
26. Li, W., Fan, J., and Woodley, D. T. (2001) Nck/Dock: An adapter between cell surface receptors and the actin cytoskeleton, *Oncogene 20*, 6403−6417.
27. Buday, L., Wunderlich, L., and Tamas, P. (2002) The Nck family of adapter proteins: Regulators of actin cytoskeleton, *Cell Signalling 14*, 723−731.
28. Braverman, L. E., and Quilliam, L. A. (1999) Identification of Grb4/Nckbeta, a src homology 2 and 3 domain-containing adapter protein having similar binding and biological properties to Nck, *J. Biol. Chem. 274*, 5542−5549.
29. Tu, Y., Li, F., and Wu, C. (1998) Nck-2, a novel Src homology2/3-containing adaptor protein that interacts with the LIM-only protein PINCH and components of growth factor receptor kinase-signaling pathways, *Mol. Biol. Cell 9*, 3367−3382.
30. Chen, M., She, H., Kim, A., Woodley, D. T., and Li, W. (2000) Nckβ adapter regulates actin polymerization in NIH 3T3 fibroblasts in response to platelet-derived growth factor bb, *Mol. Cell. Biol. 20*, 7867−7880.
31. Wei, Z., and Song, J. (2005) Molecular mechanism underlying the thermal stability and pH-induced unfolding of CHABII, *J. Mol. Biol. 348*, 205−218.
32. Braverman, L. E., and Quilliam, L. A. (1999) Identification of Grb4/Nckbeta, a src homology 2 and 3 domain-containing adapter protein having similar binding and biological properties to Nck, *J. Biol. Chem. 274*, 5542−5959.
33. Aspenstrom, P. (2002) The WASP-binding protein WIRE has a role in the regulation of the actin filament system downstream of the platelet-derived growth factor receptor, *Exp. Cell Res. 279*, 21−33.
34. Saras, J., Wollberg, P., and Aspenstrom, P. (2004) Wrch1 is a GTPase-deficient Cdc42-like protein with unusual binding characteristics and cellular effects, *Exp. Cell Res. 299*, 356−369.
35. Katoh, M. (2002) Molecular cloning and characterization of WRCH2 on human chromosome 15q15, *Int. J. Oncol. 20*, 977−982.
36. Aspenstrom, P., Fransson, A., and Saras, J. (2004) Rho GTPases have diverse effects on the organization of the actin filament system, *Biochem. J. 377* (Part 2), 327−337.
37. Shutes, A., Berzat, A. C., Cox, A. D., and Der, C. J. (2004) Atypical mechanism of regulation of the Wrch-1 Rho family small GTPase, *Curr. Biol. 14*, 2052−2056.
38. Sattler, M., Schleucher, J., and Griesinger, C. (1999) Heteronuclear multidimensional NMR experiments for the structure determination of proteins in solution employing pulsed field gradients, *Prog. NMR Spectrosc. 34*, 93−158.
39. Delaglio, F., Grzesiek, S., Vuister, G. W., Zhu, G., Pfeifer, J., and Bax, A. (1995) NMRPipe: A multidimensional spectral processing system based on UNIX pipes, *J. Biomol. NMR 6*, 277−293.
40. Johnson, B. A., and Blevins, R. A. (1994) NMRView: A computer program for the visualization and analysis of NMR data, *J. Biomol. NMR 4*, 603−614.
41. Cornilescu, G., Delaglio, F., and Bax, A. (1999) Protein backbone angle restraints from searching a database for chemical shift and sequence homology, *J. Biomol. NMR 13*, 289−302.
42. Guntert, P. (2004) Automated NMR structure calculation with CYANA, *Methods Mol. Biol. 278*, 353−378.
43. Brunger, A. T., Adams, P. D., Clore, G. M., Delano, W. L., Gros, P., Grosse- Kunstleve, R. W., Jiang, J., Kuszewski, J., Nilges, M., Pannu, N. S., Read, R. J., Rice, L. M., Simonson, T., and Warren, G. L. (1998) Crystallography & NMR system: A new software suite for macromolecular structure determination, *Acta Crystallogr. D54*, 905−921.
44. Song, J., Gilquin, B., Jamin, N., Drakopoulou, E., Guenneugues, M., Dauplais, M., Vita, C., and Menez, A. (1997) NMR solution structure of a two-disulfide derivative of charybdotoxin: Structural evidence for conservation of scorpion toxin α/β motif and its hydrophobic side chain packing, *Biochemistry 36*, 3760−3766.
45. Laskowski, R. A., Rullmannn, J. A., MacArthur, M. W., Kaptein, R., and Thornton, J. M. (1996) AQUA and PROCHECK-NMR: Program for checking the quality of protein structures solved by NMR, *J. Biomol. NMR 8*, 477−486.
46. Koradi, R., Billeter, M., and Wuthrich, K. (1996) MOLMOL: A program for display and analysis of macromolecular structures, *J. Mol. Graphics 14*, 51−55.
47. Wiseman, T., Williston, S., Brandts, J. F., and Lin, L. (1989) Rapid measurement of binding constants and heats of binding using a new titration calorimeter, *Anal. Biochem. 179*, 131−137.
48. Renzoni, D. A., Pugh, D. J. R., Siligardi, G., Das, P., Rossi, C., Waterfield, M. D., Campbell, I. D., and Ladbury, J. E. (1996) Structural and thermodynamic characterization of the interaction of the SH3 domain from Fyn with the proline-rich binding site on the p85 subunit of PI3-kinase, *Biochemistry 35*, 15646−15653.
49. Farrow, N. A., Muhandiram, R., Singer, A. U., Pascal, S. M., Kay, C. M., Gish, G., Shoelson, S. E., Pawson, T., Forman Kay, J. D., and Kay, L. E. (1994) Backbone dynamics of a free and phosphopeptide-complexed Src homology 2 domain studied by ^{15}N NMR relaxation, *Biochemistry 33*, 5984−6003.
50. Yang, D., Mok, Y. K., Forman-Kay, J. D., Farrow, N. A., and Kay, L. E. (1997) Contributions to protein entropy and heat capacity from bond vector motions measured by NMR spin relaxation, *J. Mol. Biol. 272*, 790−804.
51. Mandel, A. M., Akke, M., and Palmer, A. G., III (1995) Backbone dynamics of *Escherichia coli* ribonuclease HI: Correlations with structure and function in an active enzyme, *J. Mol. Biol. 246*, 144−163.
52. Dosset, P., Hus, J. C., Blackledge, M., and Marion, D. (2000) Efficient analysis of macromolecular rotational diffusion from heteronuclear relaxation data, *J. Biomol. NMR 16*, 23−28.
53. Fielding, L., Rutherford, S., and Fletcher, D. (2005) Determination of protein−ligand binding affinity by NMR: Observations from serum albumin model systems, *Magn. Reson. Chem. 43*, 463−470.
54. Kay, B. K., Williamson, M. P., and Sudol, M. (2000) The importance of being proline: The interaction of proline-rich motifs in signaling proteins with their cognate domains, *FASEB J. 14*, 231−241.
55. Mayer, B. J. (2001) SH3 domains: Complexity in moderation, *J. Cell Sci. 114*, 1253−1263.
56. Musacchio, A. (2002) How SH3 domains recognize proline, *Adv. Protein Chem. 61*, 211−268.
57. Zarrinpar, A., Bhattacharyya, R. P., and Lim, W. A. (2003) The structure and function of proline recognition domains, *Sci. STKE 2003*, RE8.

58. Cesareni, G., Panni, S., Nardelli, G., and Castagnoli, L. (2002) Can we infer peptide recognition specificity mediated by SH3 domains? *FEBS Lett. 513*, 38−44.
59. Larson, S. M., and Davidson, A. R. (2000) The identification of conserved interactions within the SH3 domain by alignment of sequences and structures, *Protein Sci. 9*, 2170−2180.
60. Li, S-C. (2005) Specificity and versatility of SH3 and other proline-recognition domains: Structural basis and implications for cellular signal transduction, *Biochem. J. 390*, 641−653.
61. Ball, L. J., Kuhne, R., Schneider-Mergener, J., and Oschkinat, H. (2005) Recognition of proline-rich motifs by protein−protein interaction domains, *Angew. Chem., Int. Ed. 44*, 2852−2869.
62. Venyaminov, S. Y., and Yang, J. T. (1996) Determination of protein secondary structure, in *Circular Dichroism and the Conformational Analysis of Biomolecules* (Fasman, G. D., Ed.) pp 69−107, Plenum Press, New York.
63. Farrow, N. A., Zhang, O., Forman-Kay, J. D., and Kay, L. E. (1995) Comparison of the backbone dynamics of a folded and an unfolded SH3 domain existing in equilibrium in aqueous buffer, *Biochemistry 34*, 868−878.
64. Wales, T. E., and Engen, J. R. (2006) Partial Unfolding of Diverse SH3 Domains on a Wide Timescale, *J. Mol. Biol. 357*, 1592−1604.
65. Kroenke, C. D., Loria, J. P., Larry, K. L., Rance, M., and Palmer, A. G., III (1998) Longitudinal and Transverse ^{1}H-^{15}N Dipolar/^{15}N Chemical Shift Anisotropy Relaxation Interference: Unambiguous Determination of Rotational Diffusion Tensors and Chemical Exchange Effects in Biological Macromolecules, *J. Am. Chem. Soc. 120*, 7905−7915.
66. Canet, D., Barthe, P., Mutzenhardt, P., and Roumestand, C. (2001) A comprehensive analysis of multifield ^{15}N relaxation parameters in proteins: Determination of ^{15}N chemical shift anisotropies, *J. Am. Chem. Soc. 123*, 4567−4576.
67. Houtman, J. C., Barda-Saad, M., and Samelson, L. E. (2005) Examining multiprotein signaling complexes from all angles, *FEBS Lett. 272*, 5426−5435.
68. Vondriska, T. M., Pass, J. M., and Ping, P. (2004) Scaffold proteins and assembly of multiprotein signaling complexes, *J. Mol. Cell. Cardiol. 37*, 391−397.
69. Burack, W. R., Cheng, A. M., and Shaw, A. S. (2002) Scaffolds, adaptors and linkers of TCR signaling: theory and practice, *Curr. Opin. Immunol. 14*, 312−316.
70. Mayer, B. J. (1999) Protein−protein interactions in signaling cascades, *Mol. Biotechnol. 13*, 201−213.
71. Sudol, M. (1998) Physical and functional interactions between the transactivation domain of the hematopoietic transcription factor NF-E2 and WW domains, *Oncogene 17*, 1469−1474.
72. Pawson, T. (2004) SH2 and SH3 domains: From structure to function, *Cell 116*, 191−203.
73. Donaldson, L. W., Gish, G., Pawson, T., Kay, L. E., and Forman-Kay, J. D. (2002) Structure of a regulatory complex involving the Abl SH3 domain, the Crk SH2 domain, and a Crk-derived phosphopeptide, *Proc. Natl. Acad. Sci. U.S.A. 99*, 14053−14058.
74. Machida, K., and Mayer, B. J. (2005) Critical amino acid substitutions in the Src SH3 domain that convert c-Src to be oncogenic, *Biochim. Biophys. Acta 1747*, 1−25.
75. Mayer, B. J. (1998) Protein−protein interactions in signaling cascades, *Methods Mol. Biol. 84*, 33−48.
76. Manser, E., Leung, T., Salihuddin, H., Tan, L., and Lim, L. (1993) A non-receptor tyrosine kinase that inhibits the GTPase activity of p21cdc42, *Nature 363*, 364−367.
77. Zhao, Z. S., Manser, E., and Lim, L. (2000) Interaction between PAK and nck: A template for Nck targets and role of PAK autophosphorylation, *Mol. Cell. Biol. 20*, 3906−3917.
78. Velyvis, A., Vaynberg, J., Yang, Y., Vinogradova, O., Zhang, Y., Wu, C., and Qin, J. (2003) Structural and functional insights into PINCH LIM4 domain-mediated integrin signaling, *Nat. Struct. Biol. 10*, 558−564.
79. Vaynberg, J., Fukuda, T., Chen, K., Vinogradova, O., Velyvis, A., Tu, Y., Ng, L., Wu, C., and Qin, J. (2005) Structure of an ultraweak protein−protein complex and its crucial role in regulation of cell morphology and motility, *Mol. Cell 17*, 513−523.
80. Renzoni, D. A., Pugh, D. J., Siligardi, G., Das, P., Morton, C. J., Rossi, C., Waterfield, M. D., Campbell, I. D., and Ladbury, J. E. (1996) Structural and thermodynamic characterization of the interaction of the SH3 domain from Fyn with the proline-rich binding site on the p85 subunit of PI3-kinase, *Biochemistry 35*, 15646−15653.
81. Wang, C., Pawley, N. H., and Nicholson, L. K. (2001) The role of backbone motions in ligand binding to the c-Src SH3 domain, *J. Mol. Biol. 313*, 873−887.
82. Li, M., Shi, J., Wei, Z., Teng, F. Y., Tang, B. L., and Song, J. (2004) Structural characterization of the human Nogo-A functional domains. Solution structure of Nogo-40, a Nogo-66 receptor antagonist enhancing injured spinal cord regeneration, *Eur. J. Biochem. 271*, 3512−3522.
83. Koeberle, P. D., and Bahr, M. (2004) Growth and guidance cues for regenerating axons: Where have they gone? *J. Neurobiol. 59*, 162−180.
84. Oertle, T., and Schwab, M. E. (2003) Nogo and its paRTNers, *Trends Cell Biol. 13* (4), 187−194.
85. Lee, D. H., Strittmatter, S. M., and Sah, D. W. (2003) Targeting the Nogo receptor to treat central nervous system injuries, *Nat. Rev. Drug Discovery 2*, 872−878.
86. Voeltz, G. K., Prinz, W. A., Shibata, Y., Rist, J. M., and Rapoport, T. A. (2006) A class of membrane proteins shaping the tubular endoplasmic reticulum, *Cell 124*, 573−586.

BI060091Y